FULL PAPER

WILEY Applied Organometallic Chemistry

V-N-C catalysts anchored to mesoporous Al-SBA-15 with tailorable pore sizes for the synthesis of spirooxindole dihydroquinazolinones derivatives

Javad Safaei-Ghomi [ID] | Raheleh Teymuri

Department of Organic Chemistry, Faculty of Chemistry, University of Kashan, KashanP.O. Box 87317-51167, I. R., Iran

Correspondence
Javad Safaei-Ghomi, Department of Organic Chemistry, Faculty of Chemistry, University of Kashan, Kashan, P.O. Box 87317-51167, I. R. Iran.
Email: safaei@kashanu.ac.ir

Heterogeneous nanoscale catalyst was successfully synthesized via anchoring of V-bis(2-aminobenzamide) complex on the Al-SBA-15. This modified mesoporous was identified by several characterization techniques, such as X-ray diffraction, field emission-scanning electron microscopy, Fourier transform-infrared, Brunauer–Emmett–Teller and transmission electron microscopy. V-Bis(2-aminobenzamide)@Al-SBA-15 was found to be an efficient heterogeneous catalyst for the rapid and desirable synthesis of various spirooxindole dihydroquinazolinones derivatives. In addition, the heterogeneous nanocatalyst was chemically stabilized in organic and aqueous solutions as well as can be expeditiously reused for at least seven cycles without a significant loss in catalytic activity.

KEYWORDS
aluminosilicate, dihydroquinazolinones, modified mesoporous, three-component condensation

1 | INTRODUCTION

In recent years, spirooxindole and their derivatives have attracted momentous attention due to its unequalled core structure and great biological activities, such as anticancer, anticonvulsant, fungicidal and herbicidal (Figure 1). [1–5] Spirooxindole dihydroquinazolinone is one of this class of compounds that combines two pharmacophores into one molecule, so our attention was attracted to find more potent pharmaceutical active molecules.[6] To date, many attempts have been devoted to disclose desirable protocols for the synthesis of spirooxindoles. In this line, the utilities of many catalysts, including KAl (SO$_4$)$_2$·12H$_2$O (alum),[7] 1-methylimidazolium hydrogen sulfate,[8] ethylenediamine diacetate[9] and nano CeO$_2$,[10] have been evidenced, whereas some of these experimental procedures have obvious negative aspects, such as long reaction times, low yields and harsh reaction conditions. Accordingly, to avoid these limitations, the exploration of an efficient, easily available catalyst with high catalytic activity and short reaction times for the preparation of spirooxindole dihydroquinazolinone is still favored.

Ordered mesoporous silicas such as those of M41S, SBA-n and MSU-X families discovered in the early 1990s have been regarded as a promising class of materials for catalysis and separation.[11,12] These materials serve as an exceptional choice for such applications. Moreover, they offer high specific surface areas, large and defined pore sizes, defined surface acidity, and excellent mechanical and thermal stability.[13–16] In this regard, the substituents such as aluminum, titanium and zirconium can be incorporated into the silica framework to obtain materials for applications such as catalysis and ion exchange. Among the metal-substituted mesoporous materials, aluminum-incorporated mesoporous materials have great potential in moderating acid-catalyzed reactions for large molecules.[17,18] Moreover, the addition of heteroatoms such as aluminum (with lower than silicon valence) introduces the negative charges in the silica walls that are
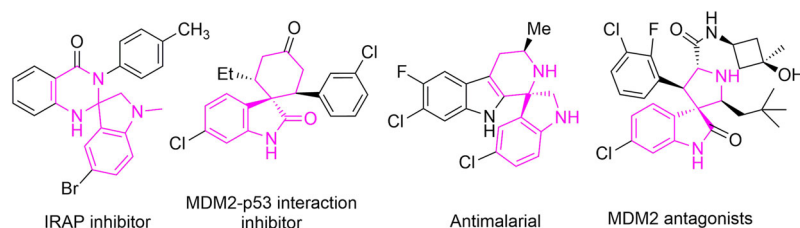
FIGURE 1 Reported biologically active spirooxindole-based molecules

compensated by protons, and generates an acidity in these systems, improving the surface properties of the final product.[19] Based on these distinctive attributes, a large number of research groups have pursued new and creative approaches toward incorporating multiple functional groups onto heterogeneous catalysts, which can catalyze multistep reaction cascades in one system or work in a cooperative manner to alter the characteristics of a single reaction.[20–29]

In the current work, the use of material with surface functional groups shows improved selectivity catalyst. Consequently, we synthesize the novel hybrid V-bis(2-aminobenzamide)@Al-SBA-15 (V-N-C@Al-SBA-15) by chloro-functionalized with employing 3-chloropropyltriethylsilane (CPTES) and anchored bis(2-aminobenzamide) on it. The synthesizing process was pursued by grafting of V (IV) to catch the desired product. Also the activity of the catalyst has been scrutinized by synthesizing spirooxindole dihydroquinazolinone derivatives (Scheme 1).

2 | EXPERIMENTAL

2.1 | Materials and apparatus

All organic materials were purchased commercially from Sigma–Aldrich and Merck, and were used without further purification. Melting points of products were determined by Electro thermal 9200. All infrared (IR) spectra were recorded by means of Fourier transform (FT)-IR Magna spectrometer 550 Nicolet using KBr plates. NMR spectra were attained in DMSO-d_6 as a solvent, and are reported as parts per million (ppm) downfield from TMS as an internal standard. The NMR spectra were obtained on a Bruker Avance-400 MHz spectrometer. The elemental analyses (C, H, N) were obtained from a Carlo ERBA Model EA 1108 analyzer. The X-ray diffraction (XRD) patterns were recorded on an X-ray diffractometer (PHILIPS, PW 1510, the Netherlands) using Cu-Kα radiation (λ = 0.154056 nm) in the range 2θ = 0–10°. Field emission-scanning electron microscopy (FE-SEM) of nanoparticles was taken on a Model FE-SEM. Transmission electron microscopy (TEM) images were performed on a Philips EM208 TEM with an accelerating voltage of 200 kV. The N_2 adsorption/desorption analysis [Brunauer–Emmett–Teller (BET)] was performed at 120°C using an automated gas adsorption analyzer (BEL SORP mini II). X-ray photoelectron spectroscopy (XPS) spectra were recorded using a ESCA System 100 spectrometer (VSW Scientific Instruments, UK).

2.2 | Preparation of Al-SBA-15

Al-SBA-15 was synthesized following published procedures.[30,31] In a classic procedure, 2 g of pluronic P123 was dissolved in 75 ml hydrochloric acid solution at pH 1.5. The solution was stirred at 40°C for 6 hr. A second solution was made by adding 3.2 ml of TEOS (tetraethylorthosilicate) and 5 ml of hydrochloric acid solution at pH 1.5 to 0.22 g of aluminum isopropoxide. This suspension was vigorously stirred in a closed flask for 1.5 hr, during which it became clear. The TEOS solution was quickly added to the surfactant solution and stirred for 20 hr at 40°C. The resulting clear suspension was transferred to a Teflon-lined stainless-steel autoclave and heated to 100°C for 20 hr. The recovered white solid was filtrated and washed three times with demineralized water and twice times with ethanol. The sample was dried overnight at 100°C. The template was removed by calcination for 10 hr at 550°C with a heating ramp of 1°C/min. The sample is designated as Al-SBA-15.

2.3 | Preparation of CPTES@Al-SBA-15

Cl-functionalized Al-SBA-15 was prepared according to the literature.[32] Typically, to a suspension of Al-SBA-15
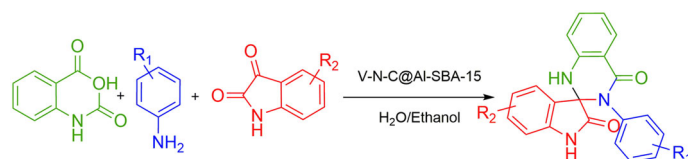
SCHEME 1 V-N-C@Al-SBA-15 catalyzed synthesis of spiro[indoline-3,2′-quinazoline]-2,4′(3′H)-dione derivatives

(5 g) in dry toluene (100 ml), (3-chloropropyl) trimethoxysilane (5 ml) was added. The mixture was subsequently refluxed at 110°C for 24 hr under inert (N_2) atmosphere. Upon completion, the obtained white participate was filtered, washed several times with toluene, and dried at 90°C overnight.

2.4 | Preparation of bis(2-aminobenzamide)

The bis(2-aminobenzamide) compound was synthesized by gradually adding 0.575 mg of 1,3–diaminopropane (6.125 mmol) in 10 ml DI water to 2.0 mg of isatoic anhydride (12.25 mmol) with continuous stirring. Effervescence was observed while warming the reaction mixture on a water bath, which ceased after 1 hr. Microcrystalline solid product was created on allowing the mixture to stand overnight. The desired product was purified and recrystallized from ethanol/water mixture.[33] The structure of the ligand was confirmed using ^{1}H-NMR and shown in Figure 2.

2.5 | Preparation of bis(2-aminobenzamide)@Al-SBA-15

The Al-SBA-15 with chloropropyl linkers (1 g) were suspended in absolute ethanol (60 ml) in a 250-ml round-bottom flask by sonication to form a uniform dispersion. Then 0.312 g (1 mmol) of the bis(2-aminobenzamide) ligand was added to the solution and the reaction mixture was refluxed for 18 hr. To remove unreacted substrate, the precipitated solid was washed repeatedly with toluene. Then it was put at a hot-air oven

at 90°C overnight to dry and furnish the functionalized Al-SBA-15.

2.6 | Preparation of V-bis(2-aminobenzamide)@Al-SBA-15

One gram of bis(2-aminobenzamide)@Al-SBA-15 was suspended in 50 ml absolute ethanol, then 0.2 g of VCl_3 was added and refluxed for 12 hr to anchor VCl_3. Upon stirring and heating to 65°C, the color of the turbid reaction mixture changed to greenish gray after 12 hr, and solid V-bis(2-aminobenzamide)@Al-SBA-15 (V-N-C @Al-SBA-15) resulted. It was washed repeatedly with ethanol and dried under vacuum.

All of the steps for the functionalization of the modified surface of mesoporous Al-SBA-15 with chloro-N,N'-(propane-1,3-diyl)bis(2-aminobenzamide) vanadium (IV) complex have been shown in Scheme 2.

2.7 | General procedure for the preparation of spiro[indoline-3,2′-quinazoline]-2,4′(3′H)-dione under mild reaction

Regularly, isatoic anhydride (1.0 mmol), aniline (1.1 mmol), isatin (1 mmol) and V-bis(2-aminobenzamide)@Al-SBA-15 as catalyst were mixed in H_2O/EtOH = 1:1 (10 ml). Aniline and isatoic anhydride were refluxed in the presence of catalyst for 10 min, followed by the addition of isatin for the desired times. As soon as the reaction was completed (monitored by thin-layer chromatography), the modified mesoporous catalyst was separated by filtration. At that instant, 10 ml ice water was added and the precipitated product
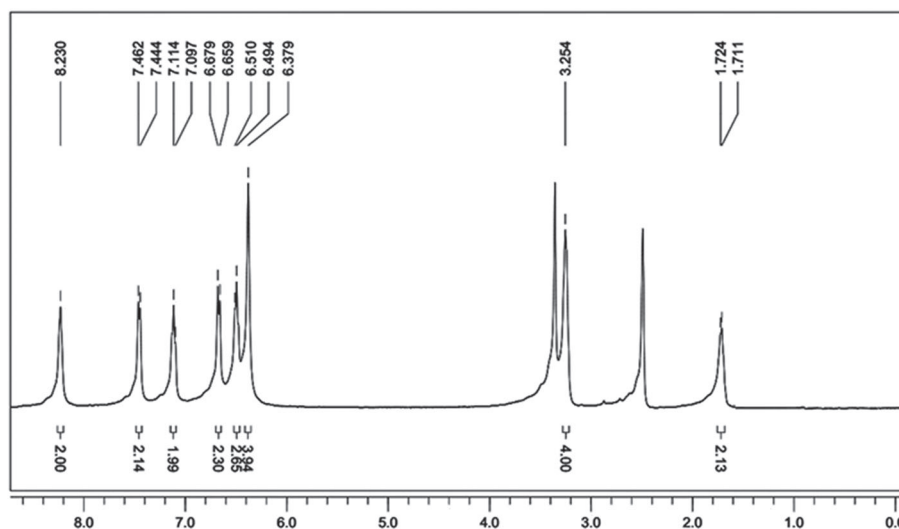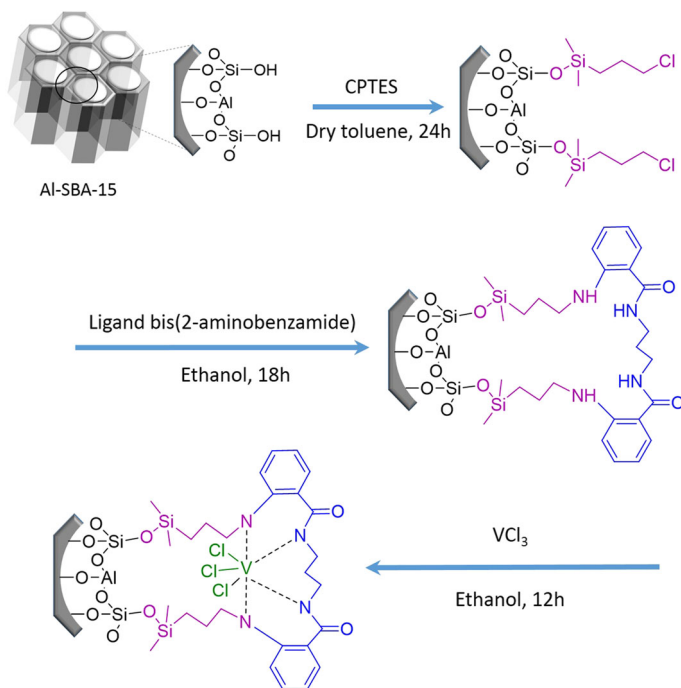

FIGURE 2 ^{1}H-NMR of bis(2-aminobenzamide) in DMSO

SCHEME 2 Grafting route for mesoporous Al-SBA-15 functionalization

was filtered. At the end of the process, the residue was recrystallized from ethanol to obtain the crude product.

2.8 | Representative spectral data of spiro[indoline-3,2′-quinazoline]-2,4′(3′H)-dione

2.8.1 | 1′H-Spiro[indoline-3,2′-quinazoline]-2,4′(3′H)-dione (4a)

m.p. 262–264°C. FT-IR (KBr) cm^{-1}: 3374, 3328, 3248, 1744, 1617, 1484, 1360, 1189, 748, 694. ^{1}H-NMR (400 MHz, DMSO-d_6): δ (ppm) 10.55 (1H, s), 7.72 (1H, s), 7.65 (1H, d, J = 7.2 Hz), 7.63 (1H, d, J = 8 Hz), 7.29 (2H, d, J = 7.6 Hz), 7.22–7.15 (2H, m), 7.00–6.98 (1H, d, J = 7.2 Hz), 6.72 (1H, t, J = 7.6 Hz), 6.66 (1H, d, J = 7.6 Hz), 6.57 (1H, t, J = 8.4 Hz). ^{13}C-NMR (100 MHz, DMSO-d_6): δ (ppm) 172.8, 169.2, 148.2, 142.3, 141.8, 134.2, 131.5, 128.2, 127.9, 125.7, 118.6, 117.2, 115.8, 114.6, 100.3. Anal. calcd for C$_{15}$H$_{11}$N$_3$O$_2$: C, 67.92; H, 4.17; N, 15.84; % found: C, 67.62; H, 4.02; N, 15.93%.

2.8.2 | 5-Chloro-1′H-spiro[indoline-3,2′-quinazoline]-2,4′(3′H)-dione (4b)

m.p. 253–255°C. FT-IR (KBr) cm^{-1}: 3435, 3278, 1738, 1639, 1613, 1511, 1480, 1359, 1190, 813, 753. ^{1}H-NMR (400 MHz, DMSO-d_6): δ 10.54 (1H, s), 7.75 (1H, s), 7.65

(1H, s), 7.33–7.30 (2H, m), 7.04 (1H, d, J = 6.8 Hz), 6.90 (1H, d, J = 7.6 Hz), 6.76 (1H, t, J = 7.2 Hz), 6.67 (1H, d, J = 6.8 Hz), 6.60 (1H, d, J = 7.6 Hz). ^{13}C-NMR (100 MHz, DMSO-d_6): δ (ppm) 171.2, 166.3, 145.9, 143.7, 133.2, 132.5, 129.4, 126.1, 124.2, 117.1, 116.4, 115.1, 110.2, 99.1. Anal. calcd for C$_{15}$H$_{10}$N$_4$O$_4$: C, 58.07; H, 3.24; N, 18.06; found: C, 57.96; H, 3.12; N, 17.92%.

2.8.3 | 3′-Benzyl-1′H-spiro[indoline-3,2′-quinazoline]-2,4′(3′H)-dione (4c)

m.p. 212–214°C. FT-IR (KBr) cm^{-1}: 3332, 1729, 1623, 1487, 1350, 1190, 750, 694. ^{1}H-NMR (400 MHz, DMSO-d_6): δ 10.32 (1H, s), 7.68 (1H, d, J = 7.6 Hz), 7.43 (1H, s), 7.32–7.21 (3H, m), 7.13 (3H, m), 6.88 (3H, m), 6.79 (1H, d, J = 8 Hz), 6.73 (1H, t, J = 7.6 Hz), 6.63 (1H, d, J = 8 Hz), 4.45 (1H, d, J = 15.6 Hz), 4.12 (1H, d, J = 15.2 Hz). ^{13}C-NMR (100 MHz, DMSO-d_6): δ (ppm) 171.3, 162.9, 143.7, 142.6, 138.1, 136.3, 131.3, 130.8, 129.3, 129.1, 128.6, 128.1, 122.8, 119.3, 118.6, 118.3, 115.2, 104.2, 46.3. Anal. calcd for C$_{22}$H$_{17}$N$_3$O$_2$: C, 74.35; H, 4.82; N, 11.82; found: C, 74.61; H, 4.80; N, 12.03%.

2.8.4 | 3′-Benzyl-5-nitro-1′H-spiro[indoline-3,2′-quinazoline]-2,4′(3′H)-dione (4d)

m.p. 289–291°C. FT-IR (KBr) cm^{-1}: 3334.13, 1727.85, 1624.61, 1488.14, 1351.01, 1191.32, 752.14, 694.56. ^{1}H-

NMR (400 MHz, DMSO-d_6): δ 10.53 (1H, s), 7.71 (1H, d, J = 7.6 Hz), 7.48 (2H, m), 7.27 (1H, m), 7.16 (4H, m), 6.87 (2H, m), 6.75 (2H, m), 6.62 (1H, d, J = 7.6 Hz), 4.67 (1H, d, J = 15.2 Hz), 3.94 (1H, d, J = 15.6 Hz). ^{13}C-NMR (100 MHz, DMSO-d_6): δ (ppm) 171.3, 163.1, 148.1, 147.8, 144.9, 137.4, 131.4, 129.7, 128.4, 127.3, 127.1, 126.5, 123.2, 118.0, 116.5, 114.1, 110.2, 105.2, 46.1. Anal. calcd for $C_{22}H_{16}N_4O_4$: C, 65.99; H, 4.02; N, 13.99; found: C, 66.10; H, 3.82; N, 13.86%.

2.8.5 | 3′-Benzyl-5-bromo-1′*H*-spiro[indoline-3,2′-quinazoline]-2,4′(3′*H*)-dione (4e)

m.p. 301–303°C. FT-IR (KBr) cm^{-1}: 3264, 2924, 1728, 1615, 1482, 1382, 1184, 751, 697, 532. ^{1}H-NMR (400 MHz, DMSO-d_6): δ 10.55 (1H, s), 7.68 (1H, d, J = 7.6 Hz), 7.44 (2H, m), 7.26 (2H, m), 7.20 (3H, m), 6.83 (2H, m), 6.71 (2H, t, J = 6.8 Hz), 6.59 (1H, d, J = 7.6 Hz), 4.62 (1H, d, J = 15.0 Hz), 4.11 (1H, d, J = 15.2 Hz). ^{13}C-NMR (100 MHz, DMSO-d_6): δ (ppm) 171.3, 163.1, 148.1, 147.8, 144.9, 137.4, 131.4, 129.7, 128.4, 127.3, 127.1, 126.5, 123.2, 118.0, 116.5, 114.1, 110.2, 105.2, 46.1. Anal. calcd for $C_{22}H_{16}N_3O_2Br$: C, 60.70; H, 3.70; N, 9.65; found: C, 6.81; H, 3.62; N, 9.44%.

2.8.6 | 3′-Phenyl-1′*H*-spiro[indoline-3,2′-quinazoline]-2,4′(3′*H*)-dione (4f)

m.p. 351–353°C. FT-IR (KBr) cm^{-1}: 3442, 3267, 1727, 1642, 1617, 1488, 1359, 1193, 749, 694.^{1}H-NMR (400 MHz, DMSO-d_6): δ 10.42 (1H, s), 7.65 (1H, d, J = 8), 7.63 (s, 1H), 7.54 (1H, d, J = 7.2 Hz,), 7.31–7.29 (1H, m), 7.20–7.15 (3H, m), 6.99 (2H, t), 7.03–6.97 (m, 2H), 6.93 (1H, t, J = 7.6 Hz), 6.73–6.68 (m, 2H), 6.64 (d, J = 7.6 Hz, 1H). ^{13}C-NMR (100 MHz, DMSO-d_6): δ (ppm) 175.67, 163.56, 146.10, 141.65, 138.08, 133.64, 130.79, 128.60, 127.61, 127.59, 127.40, 127.29, 126.47, 122.08, 117.65, 114.57, 114.08, 110.07, 76.35. Anal. calcd for $C_{21}H_{15}N_3O_2$: C, 73.89; H, 4.42; N, 12.31; found: C, 73.95; H, 4.21; N, 12.57%.

2.8.7 | 5-Bromo-3′-phenyl-1′*H*-spiro[indoline-3,2′-quinazoline]-2,4′(3′*H*)-dione (4g)

m.p. 276–277°C. FT-IR (KBr) cm^{-1}: 3401, 3236, 2893, 1735, 1612, 1522, 1485, 1277, 1180, 751.^{1}H-NMR (400 MHz, DMSO-d_6): δ 10.57 (1H, s), 7.75 (1H, s), 7.68 (1H, d, J = 6.8 Hz), 7.65 (1H, s), 7.33–7.23 (4H, m), 7.19 (1H, d, J = 6.2 Hz), 7.02 (2H, d, J = 5.6 Hz), 6.76 (1H, t,

J = 7.2 Hz), 6.69 (1H, d, J = 7.6 Hz), 6.69 (1H, d, J = 6.8 Hz). ^{13}C-NMR (100 MHz, DMSO-d_6): δ (ppm) 172.6, 163.1, 146.4, 144.8, 142.1, 137.1, 131.7, 131.1, 128.7, 126.8, 126.3, 124.7, 118.2, 115.6, 114.1, 110.7, 106.2. Anal. calcd for $C_{21}H_{14}N_3O_2Br$: C, 61.12; H, 3.33; N, 9.72; found: C, 61.10; H, 3.37; N, 9.66%.

2.8.8 | 5-Chloro-3′-phenyl-1′*H*-spiro[indoline-3,2′-quinazoline]-2,4′(3′*H*)-dione (4h)

m.p. 194–195°C. FT-IR (KBr) cm^{-1}: 3338, 3240, 2922, 1749, 1615, 1521, 1483, 1278, 1185, 1089, 752, 695. ^{1}H-NMR (400 MHz, DMSO-d_6): δ 11.14 (1H, s), 8.39 (1H, s), 8.10 (1H, d, J = 8.2 Hz), 7.76 (1H, s), 7.73 (1H, d, J = 7.8 Hz), 7.39 (1H, t, J = 6.8 Hz), 7.21–7.13 (4H, m), 7.10 (1H, d, J = 6.8 Hz), 6.86–6.79 (2H, m), 6.70 (1H, d, J = 8.2 Hz). ^{13}C-NMR (100 MHz, DMSO-d_6): δ (ppm) 174.3, 163.2, 145.5, 143.1, 136.9, 132.5, 131.4, 129.1, 128.2, 127.1, 126.4, 125.5, 123.1, 119.0, 115.5, 115.1, 111.2, 76.2, 46.1. Anal. calcd for $C_{21}H_{14}N_3O_2Cl$: C, 68.13; H, 3.63; N, 10.83; found: C, 68.05; H, 3.49; N, 10.67%.

2.8.9 | 5-Nitro-3′-phenyl-1′*H*-spiro[indoline-3,2′-quinazoline]-2,4′(3′*H*)-dione (4i)

m.p. 276–278°C. FT-IR (KBr) cm^{-1}: 3337, 3243, 2925, 1752, 1616, 1522, 1486, 1275, 1188, 1087, 748, 696. ^{1}H-NMR (400 MHz, DMSO-d_6): δ 11.16 (1H, s), 8.40 (1H, s), 8.11 (1H, d, J = 8.4 Hz), 7.77 (1H, s), 7.70 (1H, d, J = 7.6 Hz), 7.35 (1H, t, J = 6.8 Hz), 7.25–7.17 (4H, m), 7.03 (1H, d, J = 6.8 Hz), 6.87–6.80 (2H, m), 6.71 (1H, d, J = 8 Hz). ^{13}C-NMR (100 MHz, DMSO-d_6): δ (ppm) 170.3, 162.2, 147.8, 145.6, 143.9, 138.4, 132.5, 131.3, 129.0, 127.6, 127.1, 124.3, 119.4, 115.4, 113.6, 110.2, 107.8. Anal. calcd for $C_{21}H_{14}N_4O_4$: C, 68.75; H, 3.67; N, 10.93; found: C, 68.68; H, 3.94; N, 10.71%.

2.8.10 | 3′-(4-chlorophenyl)-1′*H*-Spiro[indoline-3,2′-quinazoline]-2,4′(3′*H*)-dione (4j)

m.p. 265–267°C. FT-IR (KBr) cm^{-1}: 3256, 1726, 1644, 1615, 1489, 1357, 1149, 750. ^{1}H-NMR (400 MHz, DMSO-d_6): δ 10.36 (s, 1H), 7.69 (s, 1H), 7.60(d, 1H, J = 7.4 Hz), 7.57 (d, 1H, J = 7.4 Hz), 7.30–7.26 (m, 3H), 7.18 (t, 1H, J = 7. Hz), 7.03–6.93 (m, 3H), 6.84–6.79 (m, 3H). ^{13}C-NMR (100 MHz, DMSO-d_6): δ (ppm) 174.3, 163.2, 145.5, 143.1, 136.9, 132.5, 131.4, 129.1, 128.2, 127.1, 126.4, 125.5, 123.1, 119.0, 115.5, 115.1, 111.2, 76.2,

46.1. Anal. calcd for $C_{21}H_{14}N_3O_2Cl$: C, 68.13; H, 3.63; N, 10.83; found: C, 68.25; H, 3.41; N, 10.77%.

2.8.11 | 3′-(4-bromophenyl)-1′*H*-Spiro[indoline-3,2′-quinazoline]-2,4′(3′*H*)-dione (4k)

m.p. 212–214°C. FT-IR (KBr) cm^{-1}: 3448, 3271, 2923, 1726, 1642, 1615, 1512, 1360, 1193, 751. ^{1}H-NMR (400 MHz, DMSO-d_6): δ 10.52 (s, 1H), 7.68 (d, 1H, $J = 7.2$ Hz), 7.59 (s, 1H), 7.57 (d, 1H, $J = 7.4$ Hz), 7.45 (d, 2H, $J = 8.2$ Hz), 7.29 (t, 1H, $J = 7.4$ Hz), 7.18 (t, 1H, $J = 7.8$ Hz), 6.96–6.89 (m, 3H), 6.77–6.68 (m, 3H). ^{13}C-NMR (100 MHz, DMSO-d_6): δ (ppm) 77.2, 109.8, 113.5, 114.8, 117.6, 120.3, 121.4, 127.1, 127.6, 128.0, 131.2, 131.8, 133.1, 134.6, 137.8, 142.2, 146.7, 163.9, 175.7. Anal. calcd for $C_{21}H_{14}N_3O_2Br$: C, 61.12; H, 3.26; N, 9.72; found: C, 61.03; H, 3.28; N, 9.83%.

2.8.12 | 5-Bromo-3′-(4-bromophenyl)-1′*H*-spiro[indoline-3,2′-quinazoline]-2,4′(3′*H*)-dione (4l)

m.p. 296–298°C. FT-IR (KBr) cm^{-1}: 3268, 2924,1738, 1646, 1615, 1485, 1355, 1275, 1191, 753. 532. ^{1}H-NMR (400 MHz, DMSO-d_6): δ 10.62 (1H, s), 7.81 (1H, s), 7.72 (1H, s), 7.66 (1H, d, $J = 7.6$ Hz), 7.46 (2H, d, $J = 8$ Hz), 7.36 (1H, t, $J = 8$ Hz), 7.32 (2H, t, $J = 7.2$ Hz), 6.99 (1H, d, $J = 7.6$ Hz), 6.77 (1H, t, $J = 7.2$ Hz), 6.69 (1H, d, $J = 8$ Hz), 6.64 (1H, d, $J = 8.4$ Hz). ^{13}C-NMR (100 MHz, DMSO-d_6): δ (ppm) 171.2, 162.7, 148.1, 141.2, 139.6, 134.1, 133.6, 133.1, 132.4, 130.5, 129.4, 128.4, 123.8, 122.3, 120.1, 176.4, 115.1, 113.6, 107.8. Anal. calcd for $C_{21}H_{13}N_3O_2Br_2$: C, 51.69; H, 2.56; N, 8.22; found: C, 51.44; H, 2.63; N, 8.14%.

2.8.13 | 5-Bromo-3′-(*p*-tolyl)-1′*H*-spiro[indoline-3,2′-quinazoline]-2,4′(3′*H*)-dione (4m)

m.p. 153–155°C. FT-IR (KBr) cm^{-1}: 3443, 1751, 1610, 1514, 1486, 1337, 1249, 1188, 1083. 751. ^{1}H-NMR (400 MHz, DMSO-d_6): δ 10.51 (s, 1H), 7.78 (s, 1H), 7.61 (m, 2H), 7.29–7.31 (m, 2H), 7.00 (d, 1H, $J = 7.8$ Hz), 6.86 (d, 2H, $J = 6.7$ Hz), 6.72 (t, 1H), 6.66 (d, 1H, $J = 7.7$ Hz), 6.58 (d, 1H, $J = 8.2$ Hz), 2.11 (s, 3H). ^{13}C-NMR (100 MHz, DMSO-d_6): δ (ppm) 22.0, 77.3, 111.9, 114.6, 114.7, 114.9, 117.8, 126.3, 128.5, 128.3, 131.4, 133.7, 134.1, 135.4, 136.6, 141.7, 145.9, 162.6, 176.3. Anal. calcd for $C_{22}H_{16}N_3O_2Br$: C, 60.84; H, 3.71; N, 9.67; found: C, 60.96; H, 3.58; N, 10.02%.

2.8.14 | 5-Nitro-3′-(*p*-tolyl)-1′*H*-spiro[indoline-3,2′-quinazoline]-2,4′(3′*H*)-dione (4n)

m.p. 171–173°C. FT-IR (KBr) cm^{-1}: 3440, 1750, 1612, 1516, 1483, 1338, 1252, 1188, 1085. 752. ^{1}H-NMR (400 MHz, DMSO-d_6): δ 11.13 (1H, s), 8.40 (1H, s), 8.12 (1H, dd, $J = 6.8$, 1.6 Hz), 7.74 (1H, s), 7.69 (1H, d, $J = 7.6$), 6.34 (1H, t), 7.03 (2H, d, $J = 8.4$ Hz), 6.90 (2H, d, $J = 8.4$ Hz), 6.86 (1H, d, $J = 8.4$ Hz), 6.80 (1H, t, $J = 7.6$ Hz), 6.69 (1H, d, $J = 8$ Hz), 2.17 (1H, s). ^{13}C-NMR (100 MHz, DMSO-d_6): δ (ppm) 173.3, 165.2, 151.6, 149.3, 146.2, 138.8, 132.1, 134.6, 133.5, 132.1, 130.8, 129.2, 127.4, 118.1, 116.9, 115.2, 110.7, 107.9, 23.5. Anal. calcd for $C_{22}H_{16}N_4O_4$: C, 65.99; H, 4.02; N, 13.99; found: C, 65.86; H, 3.77; N, 13.69%.

3 | RESULTS AND DISCUSSION

The FT-IR spectra of bis(2-aminobenzamide), Al-SBA-15, CTPES@Al-SBA-15, bis(2-aminobenzamide)@Al-SBA-15, V-bis(2-aminobenzamide)@Al-SBA-15 are shown in Figure 3. The peaks at 600–1200 cm^{-1} can be attributed to the vibration of Si–O groups in the mesoporous silica framework. The absorption bands of Al-SBA-15-based materials at 1078, 802 and 460 cm^{-1} are attributed to the Si–O–Si anti-stretching vibration, the Si–O–Si stretching vibration, and the bending vibration of Si–O, respectively. The silanol groups of pure Al-SBA-15 present a characteristic weak peak at 956 cm^{-1}. Because of the functionalization of Al-SBA-15 with CPTES (Figure 3c), the weak peak declines and even disappears, signifying the formation of –Si–O– bands. This happens due to the reaction between the silanol groups of Al-SBA-15 and $(C_2H_5O)_3Si–$ groups of silylation reagent.[34] Therefore, weaker vibration intensity in the FT-IR spectra is observed possibly due to decrease of silanol groups. The characteristic bands at 2893 and 2892 cm^{-1} were associated with C-H stretching (Figure 4c).[35] The signals that appeared at 2892 cm^{-1} and 2993 cm^{-1} in curve 'c' indicated the existence of the organic propylchloride moiety in the Al-SBA. The absorption peaks at 3477, 3298, 1629 and 1546 were observed and attributed to the characteristic peaks of bis(2-aminobenzamide), due to the presence of the NH$_2$, C=O bonds. Accordingly, these signals at 1546 cm^{-1}, 1629 cm^{-1} and 3298 in curve 'd' show the successful attachment of bis(2-aminobenzamide) to SBA-15. After bis(2-aminobenzamide) coordinated with V, this IR absorption peak shifted from 1629 to 1646 cm^{-1}, which is indicative of the formation of a V–ligand bond. The results above imply the presence of bis(2-aminobenzamide) bonded on the surface of Al-SBA-15,
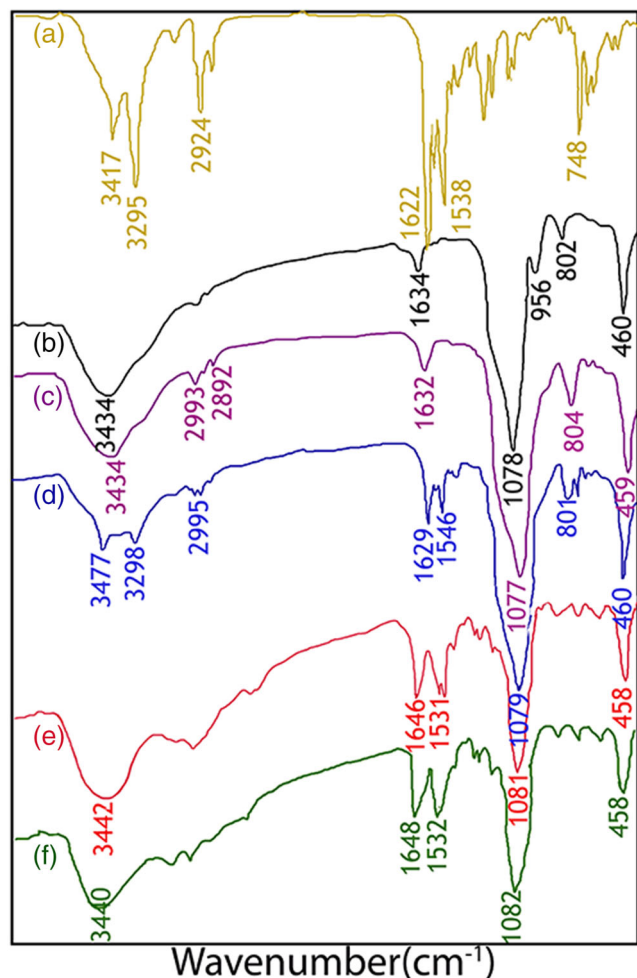
FIGURE 3 Fourier transform-infrared (FT-IR) spectra of: (a) bis(2-aminobenzamide); (b) Al-SBA-15; (c) CPES@Al-SBA-15; (d) bis(2-aminobenzamide)@Al-SBA-15; (e) V-bis(2-aminobenzamide)@Al-SBA-15; and (f) the used V-bis(2-aminobenzamide)@Al-SBA-15
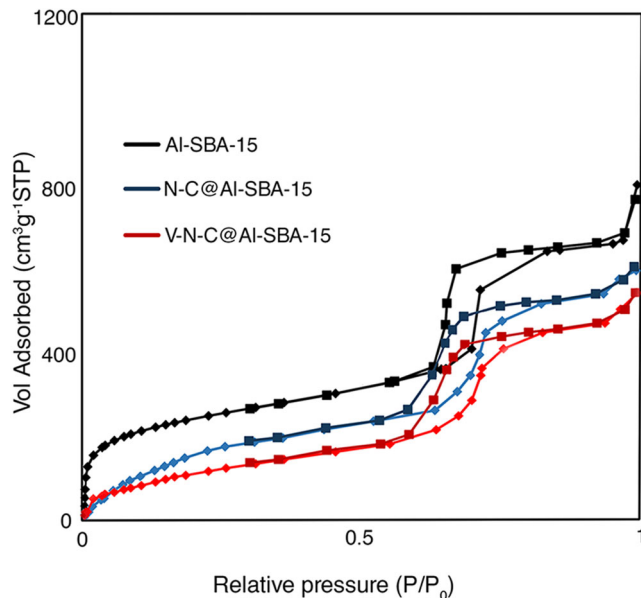

FIGURE 4 N_2 adsorption–desorption isotherms of Al-SBA-15, N-C@Al-SBA-15, V-N-C@Al-SBA-15

TABLE 1 Structural and textural parameters of SBA-15, N-C@Al-SBA-15 and V-N-C@Al-SBA-15

Sample	BET surface area (m²/g)	Pore diameter (BJH) (nm)	Total pore volume (m³/g)
Al-SBA-15	873	5.618	1.226
N-C@Al-SBA-15	549	3.461	0.475
V-N-C@Al-SBA-15	410	3.112	0.319

BET, Brunauer–Emmett–Teller; BJH, Barrett–Joyner–Halenda.

and that the molecular structure of these functional moieties can be perfectly retained in the complex of V-bis(2-aminobenzamide)@Al-SBA-15.

The N_2 adsorption/desorption isotherms and pore-size distribution curves of the samples are displayed in Figure 4. As shown in Figure 4, all the isotherms exhibited a typical type IV isotherm with an H_1 hysteresis loop starting from $P/P_0 = 0.6$. This is characteristic of mesoporous Al-SBA-15 with ordered pore structures, which is quite important to disperse and stabilize the supported vanadium species. Compared with the BET surface area (873 m²/g) of Al-SBA-15, the surface area of V-N-C@Al-SBA-15 was decreased to 410 m²/g after Al-SBA-15 was functionalized. Table 1 displays the narrow pore size distribution centred on 5.618, 3.461 and 3.112 nm for Al-SBA-15, N-C@Al-SBA-15 and V-N-C@Al-SBA-15 samples, respectively. N-C@Al-SBA-15 represent a smaller pore size than the parent Al-SBA-15 due to the

incorporation of bis(2-aminobenzamide) into the pore channels. The even smaller pore size of V-N-C@Al-SBA-15 suggested the distribution of vanadium inside the pore channels.

These results are in excellent agreement with the fact that the surface of mesoporous Al-SBA-15 has been successfully modified by bis(2-aminobenzamide). V species have entered into the channels of the Al-SBA-15 materials, resulting in the decrease in its pore size.

In order to obtain the morphology and particle size of nanoparticles, FE-SEM images of the mesopores were obtained and are presented in Figure 5. As shown in the FE-SEM images of Figure 5(a), the Al-SBA-15 sample is that with the bagel-shaped particles with relatively uniform sizes. After being functionalized with V-N-C@Al-SBA-15, the shape of Al-SBA-15 is noticeably unchanged (Figure 5b).
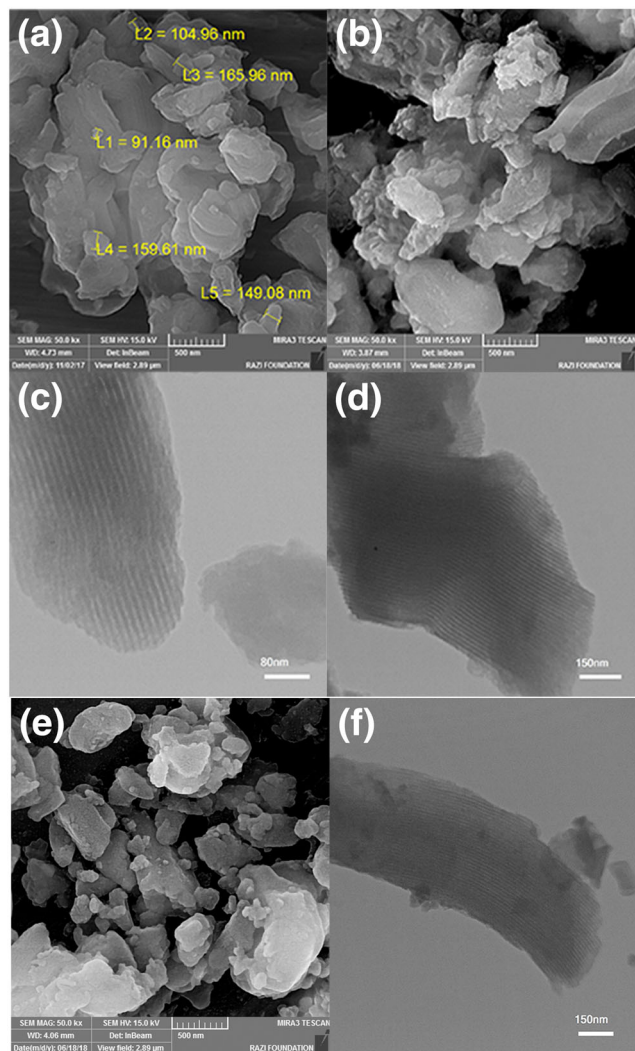
FIGURE 5 Field emission-scanning electron microscopy (FE-SEM) images of: (a) Al-SBA-15; (b) V-N-C@Al-SBA-15; (e) the used V-N-C@Al-SBA-15; and transmission electron microscopy (TEM) image of: (c) Al-SBA-15; (d) V-N-C@Al-SBA-15; (f) the used V-N-C@Al-SBA-15

FIGURE 6 Low-angle X-ray diffraction (XRD) patterns of Al-SBA-15 and V-N-C@Al-SBA-15

The TEM images of the Al-SBA-15 (Figure 5c) and V-N-C@Al-SBA-15 (Figure 5d) samples reveal that the porous structure was not disrupted after the post-grafting synthesis. Accordingly, it can be concluded that the regularity of the mesoscopic channels was well retained after the modification procedure, which further highlights the stability of the catalyst during the functionalization process. These observations are also in very good agreement with the data obtained from the small-angle XRD and nitrogen adsorption–desorption analyses.

The evaluation of the used catalyst structure by FE-SEM and TEM evidences that the morphology of the catalyst remained unchanged after the 5th cycle (Figure 5e and f).

The small-angle XRD patterns of Al-SBA-15 and V-N-C@Al-SBA-15 are shown in Figure 6. The Bragg peaks

in the 2q range of 0–2, which can be indexed as (1 0 0), (1 1 0) and (2 0 0) reflections of the two-dimensional hexagonal structure of the SBA-15 material. As can be seen the regularity of Al-SBA-15 is decreased.

The ordered structure of V-N-C@Al-SBA-15 has remained intact, as supported by the XRD results. Also there is no major change in the crystallinity of Al-SBA-15 after functionalization and V immobilization. Furthermore, the diffraction peaks of V species cannot be detected, which also shows that the V species were immobilized into the pore channels of Al-SBA-15 in the atom dispersion, and no crystal V species existed in the sample.

Figure 7 shows the XPS wide scan spectrum; the presence of V 2p, C 1s, N 1s and O 1s signals further confirms the composition of V-N-C @Al-SBA-15.

The result (Figure 7a) demonstrated that all the V species in the V-N-C @Al-SBA-15 catalyst were present in the V^{4+} state, corresponding to the binding energies of 517.2 and 523.50 eV in V 2p3/2 and V 2p1/2 levels, suggesting that the V (IV) species deposited on V-N-C @Al-SBA-15 support.[36–38] To determine the chemical microenvironment of the organic functional groups in the mesoporous silica, the electronic states of carbon, nitrogen and oxygen elements were also analyzed by the XPS spectrum. As shown in Figure 7(b), the C 1s spectra clearly indicated the V-N-C @Al-SBA-15 sample has peaks at 284.8 eV and 286.9 eV corresponding to the non-oxygenated carbon in the phenyl ring and C=O in the amide group. Meanwhile, two peaks with binding energy at 400.7 eV could be observed in N 1s spectra of the V-N-C @Al-SBA-15 sample (Figure 7c).
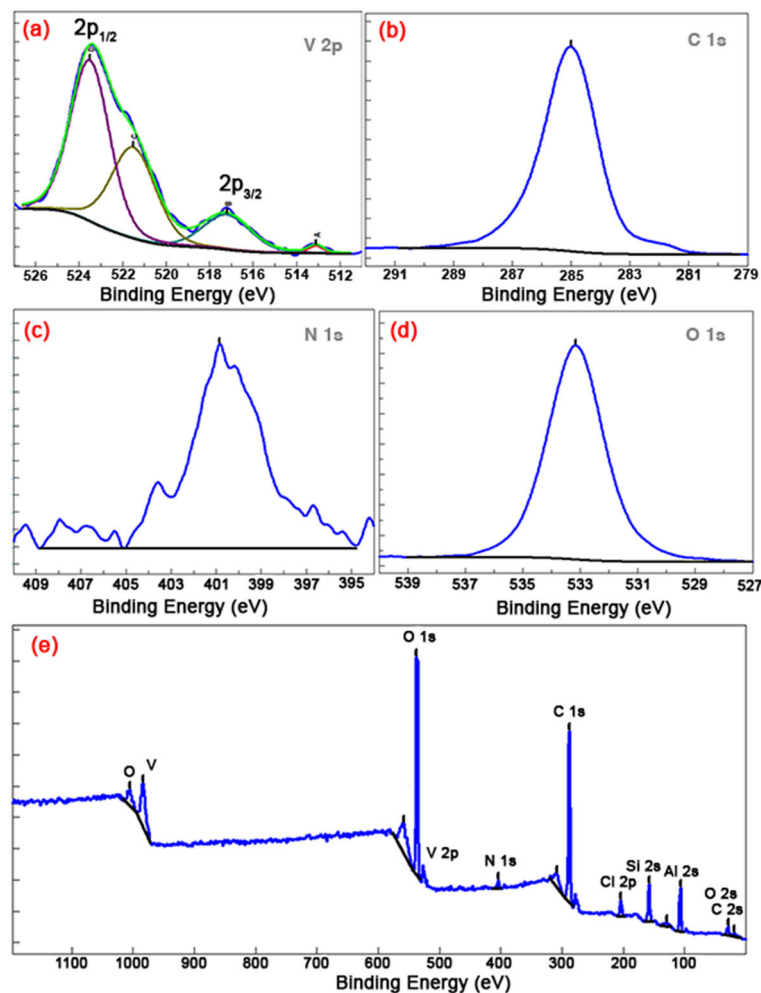
FIGURE 7 High-resolution X-ray photoelectron spectroscopy (XPS) spectra of: (a) V 2P; (b) C 1s; (c) N 1s; (d) O 1s; and (e) XPS survey spectrum of V-N-C@Al-SBA-15

This peak shows binding energy for the amide group (CO–NH-C).[39,40]

The elemental composition of V-N-C @Al-SBA-15 was shown by energy-dispersive X-ray spectroscopy (EDS) spectrum (Figure 8). Elemental analysis results showed that the carbon, nitrogen, oxygen, aluminum, silicon
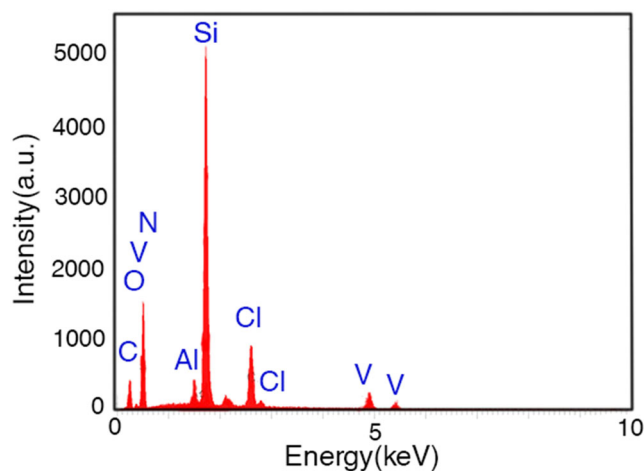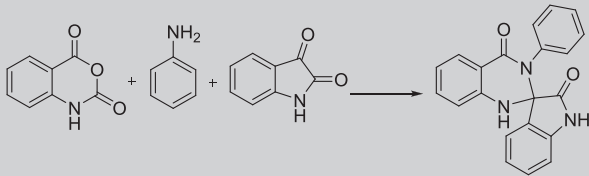

FIGURE 8 Energy-dispersive X-ray spectroscopy (EDS) of V-N-C@Al-SBA-15

and vanadium amounts of the V-N-C @Al-SBA-15 were 24.14, 9.67, 33.91, 2.10, 19.40, 3.62 (wt %).

As a result of our great interest in preparation of heterocyclic compounds by applying heterogeneous catalysts,[41,42] herein we wish to report an efficient procedure to synthesize spiro[indoline-3,2′-quinazoline] derivatives through a three-component one-pot condensation of isatoic anhydride, isatins and primary amines/or ammonium acetate using V-N-C@Al-SBA-15 as catalyst (Scheme 1). Beforehand, the reaction of isatoic anhydride, isatin and aniline was picked out as a model reaction. And now the effect of experimental factors comprising type and amount of catalyst and solvent were investigated to find the best conditions for this reaction, and the results are listed in Table 2. When the reaction was carried out in EtOH/H_2O, the expected product was obtained in high yield (95%) and with better reaction times compared with other organic solvents (Table 2, entry 10). With non-polar dichloromethane, the desired adduct was produced in trace amounts, likely due to insolubility of the isatoic anhydride.

According to the table, comparison of this entry with entries 10–15 of Table 2 reveals that the V-N-C@Al-

TABLE 2 The effect of reaction conditions on the synthesis of spiro[indoline-3,2′-quinazoline]-2,4′(3′H)-dione under various conditions

Entry	Solvent (condition)	Catalyst	Time (min)	Yield[a] (%)
1	Solvent-free	V-N-C@Al-SBA-15 (0.03 g)	120	42
2	Water (reflux)	V-N-C @Al-SBA-15 (0.03 g)	125	50
3	DCM (reflux)	V-N-C@Al-SBA-15 (0.03 g)	150	trace
4	Acetone (reflux)	V-N-C@Al-SBA-15 (0.03 g)	150	20
5	Acetonitrile (reflux)	V-N-C@Al-SBA-15 (0.03 g)	125	35
6	Methanol (reflux)	V-N-C @Al-SBA-15 (0.03 g)	100	72
7	Ethanol (reflux)	V-N-C@Al-SBA-15 (0.03 g)	75	74
8	Ethanol/H$_2$O (1:1) (reflux)	V-N-C@Al-SBA-15 (0.02 g)	70	84
9	Ethanol/H$_2$O (2:1) (reflux)	V-N-C@Al-SBA-15 (0.03 g)	70	88
10	Ethanol/H$_2$O (1:1) (reflux)	V-N-C@Al-SBA-15 (0.03 g)	70	95
11	Ethanol (reflux)	Al-SBA-15 (0.03 g)	120	62
12	EtOH (reflux)	KAl (SO$_4$)$_2$·12H$_2$O(alum) (0.4 g)	420	91
13	Acetonitrile	1-Methylimidazolium hydrogen sulfate (1.59 ml)	100	94
14	H$_2$O (reflux)	Ethylenediamine diacetate (0.036)	300	94
15	Ethanol/H$_2$O (1:1) (reflux)	nano CeO$_2$ (5 mol%)	240	85

[a]Isolated yields.

SBA-15 is the most efficient catalyst for the synthesis of spiro[indoline-3,2′-quinazoline] derivatives.

The optimized quantity of V-N-C@Al-SBA-15 for this synthesis is 0.03 g (Table 2, entry 10).
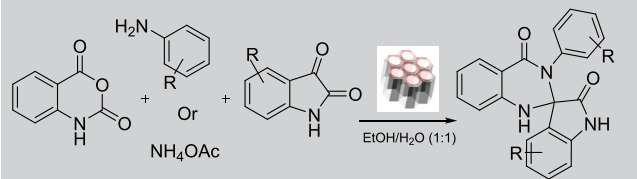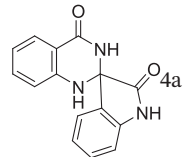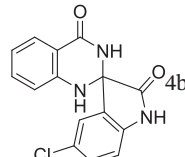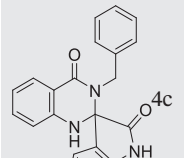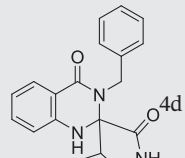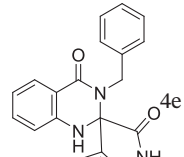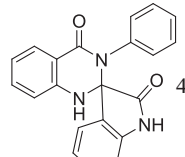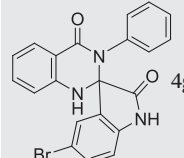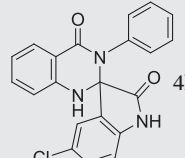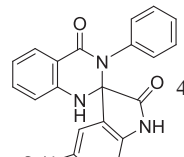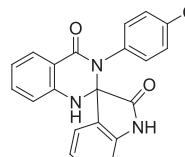
Various spiro[indoline-3,2′-quinazoline] were prepared by V-N-C @Al-SBA-15 using the obtained optimized conditions (Table 3).

These results indicate the fact that the use of as low as 0.03 g of V-N-C@Al-SBA-15 exhibits marked efficiency on all of the aliphatic and aromatic amines tested under desired reaction conditions (Table 3). As shown in Table 3, the product **4c** was formed through the reaction between isatoic anhydride, benzylamine and isatin in high yield. This reaction was fairly general, clean, extremely rapid and efficient under the optimized reaction conditions in the presence of V-N-C @Al-SBA-15. All novel and known products were characterized by comparing their physical data, ^{1}H-NMR, ^{13}C-NMR, FT-IR spectroscopy and elemental analysis spectra.

On the basis of the point mentioned above, a reasonable mechanism for the preparation of spiro[indoline-3,2′-quinazoline]-2,4′(3′H)-dione derivatives by the V-N-C@Al-SBA-15 is suggested in Scheme 3. The first point was t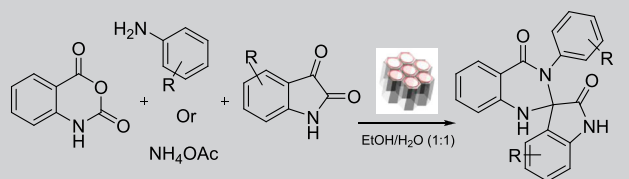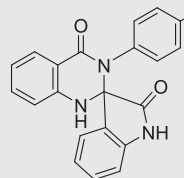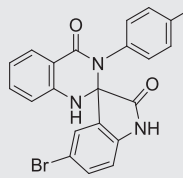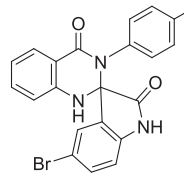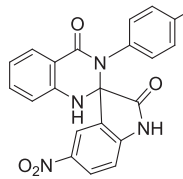he interaction of V-N-C@Al-SBA-15 as a catalyst and isatoic anhydride to produce a reactive intermediate I. And now, the N-nucleophilic primary amine attacks on the carbonyl unit of I to produce a reactive intermediate II, which in turn affords III through decarboxylation reaction. Subsequently, the proton transfer of III affords 2-amino-N-substituted-amide IV. Also the reaction of an activated isatin with IV proceeds to produce the imine intermediate V. The part of the amide functional group in intermediate IV could be formed using tautomerism phenomenon in the presence of V-N-C@Al-SBA-15. Accordingly, intermediate VI could be prepared by an intermolecular nucleophilic attack of the amide nitrogen on activated imine carbon, followed by a 1,5-proton transfer to yield the final spiro[indoline-3,2′-quinazoline]-2,4′(3′H)-dione as the concluding product. Without a catalyst, the reaction occurred under the conditions to give 18% yield. Active sites on the porous surface of the catalyst were considerably increased by adding the catalyst, and reached the best yield value (95%) with 0.03 g of V-N-C@Al-SBA-15 catalyst. Also, the results established the superior catalytic activity of this catalyst compared with some conventional catalysts, for example bare Al-SBA-15 (Table 2, entry 11). For the aforementioned mechanism, the significant roles of V-N-C@Al-SBA-15
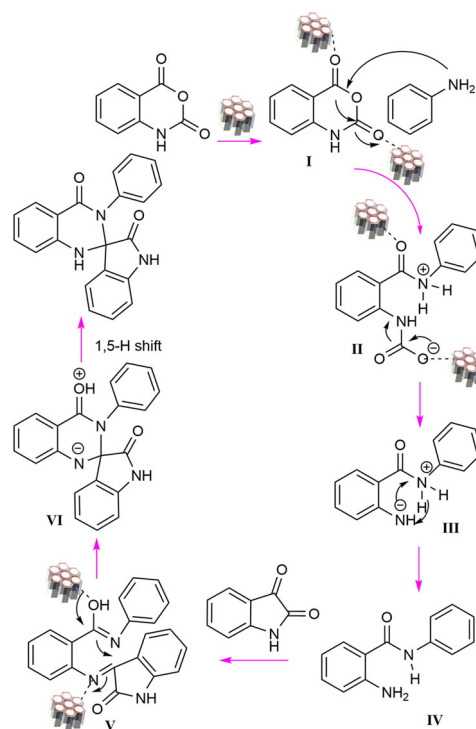
TABLE 3 Synthesis of monosubstituted spiro[indoline-3,2′-quinazoline]-2,4′(3′H)-dione using V-N-C@Al-SBA-15

Time/yield% m.p.[Ref]	Time/yield% m.p.[Ref]
4a	4b
38 min/95	35 min/96
262–2648[9]	253–255
4c	4d
47 min/97	46 min/96
212–2148[9]	289–291
4e	4f
44 min/95	70 min/95
301–303	251–2537[8]
4g	4h
65 min/94	62 min/94
276–2778[9]	194–1959[10]
4i	4j
50 min/95	52 min/90
276–278	265–2676[7]

(Continues)

TABLE 3 (Continued)

Time/yield% m.p.[Ref]	Time/yield% m.p.[Ref]
4k	4l
80 min/89	72 min/90
212–2146[7]	296–2987[8]
4m	4n
58 min/94	48 min/95
153–1559[10]	171–1739[10]

SCHEME 3 Proposed reaction mechanism for the formation of substituted spiro[indoline-3,2′-quinazoline]-2,4′(3′H)-diones using V-N-C@Al-SBA-15
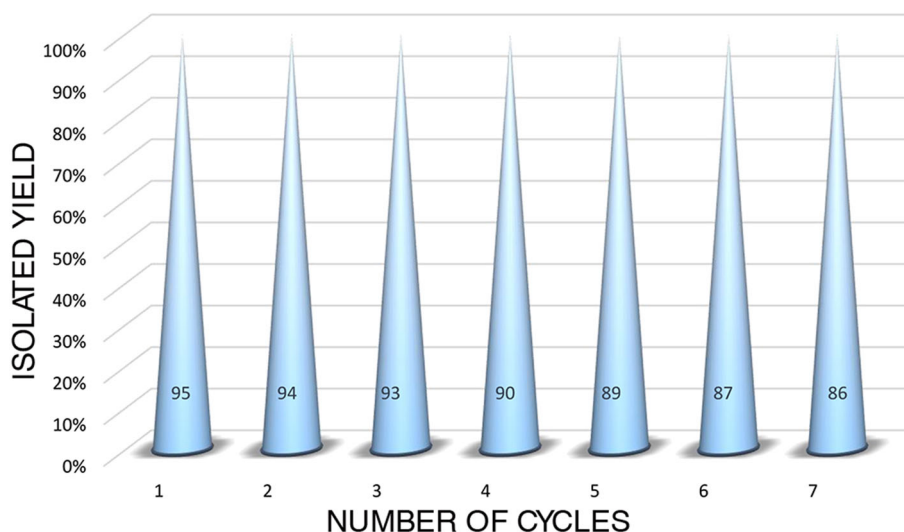
FIGURE 9 Recyclability study of V-N-C@Al-SBA-15 as a heterogeneous catalyst for the reaction of isatoic anhydride, isatin and aniline under optimized conditions

are activation of carbonyl groups and efficient development of the reaction on its high surface area.

The catalyst exhibited reusability and high stability, which emerged from the strong interaction of vanadium atom and amine groups. Investigating the reusability of the catalyst for seven reaction runs demonstrated only 7% decrease of the yield of the desired product, indicating the excellent reusability of the catalyst (Figure 9).

4 | CONCLUSIONS

To recap briefly, we have reported a selective and efficient method for the synthesis of spiro[indoline-3,2′-quinazoline]-2,4′(3′H)-dione derivatives via three-component one-pot condensation of isatoic anhydride, isatin and primary amines/or ammonium acetate using V-N-C@Al-SBA-15 as a novel catalyst. The current method provides obvious positive points, such as environmental friendliness, significantly shorter reaction time, markedly excellent yields and simple workup procedure. In our opinion, we expect this method will find extensive applications in the field of combinatorial chemistry and diversity-oriented synthesis.

ORCID

Javad Safaei-Ghomi https://orcid.org/0000-0002-9837-4478

REFERENCES

[1] B. Yu, D.-Q. Yu, H.-M. Liu, *Eur. J. Med. Chem.* **2015**, *97*, 673.

[2] R. Rios, *Chem. Soc. Rev.* **2012**, *41*, 1060.

[3] M. Rottmann, C. McNamara, B. K. Yeung, M. C. Lee, B. Zou, B. Russell, P. Seitz, D. M. Plouffe, N. V. Dharia, J. Tan, *Science* **2010**, *329*, 1175.

[4] Y. Zhao, S. Yu, W. Sun, L. Liu, J. Lu, D. McEachern, S. Shargary, D. Bernard, X. Li, T. Zhao, *J. Med. Chem.* **2013**, *56*, 5553.

[5] Z. Hosseinzadeh, A. Ramazani, N. Razzaghi-Asl, *Curr. Org. Chem.* **2018**, *22*, 2256.

[6] G. S. Singh, Z. Y. Desta, *Chem. Rev.* **2012**, *112*, 6104.

[7] M. Dabiri, A. A. Mohammadi, H. Qaraat, *Monatsh. Chem.* **2009**, *140*, 401.

[8] H. Kefayati, M. Vazifeh, R. Kazemi-Rad, *J. Chin. Chem. Soc.* **2013**, *60*, 1197.

[9] M. Narasimhulu, Y. R. Lee, *Tetrahedron* **2011**, *67*, 9627.

[10] J. Zhang, J. Zhao, L. Wang, J. Liu, D. Ren, Y. Ma, *Tetrahedron* **2016**, *72*, 936.

[11] C. T. Kresge, M. E. Leonowicz, W. J. Roth, J. C. Vartuli, J. S. Beck, *Nature* **1992**, *359*, 710.

[12] J. Beck, J. Vartuli, W. J. Roth, M. Leonowicz, C. Kresge, K. Schmitt, C. Chu, D. H. Olson, E. Sheppard, S. McCullen, *J. Am. Chem. Soc.* **1992**, *114*, 10 834.

[13] B. J. Scott, G. Wirnsberger, G. D. Stucky, *Chem. Mater.* **2001**, *13*, 3140.

[14] A. Taguchi, F. Schüth, *Microporous Mesoporous Mater.* **2005**, *77*, 1.

[15] J. Taran, A. Ramazani, H. Aghahosseini, F. Gouranlou, R. Tarasi, M. Khoobi, S. W. Joo, *Phosphorus, Sulfur Silicon Relat. Elem.* **2017**, *192*, 776.

[16] S. F. Motevalizadeh, M. Alipour, F. Ashori, A. Samzadeh-Kermani, H. Hamadi, M. R. Ganjali, H. Aghahosseini, A.

Ramazani, M. Khoobi, E. Gholibegloo, *Appl. Organomet. Chem.* **2018**, *32*, e4123.

[17] M. D. Gracia, A. M. Balu, J. M. Campelo, R. Luque, J. M. Marinas, A. A. Romero, *Appl. Catal. A General* **2009**, *371*, 85.

[18] J. A. Melero, J. M. Arsuaga, P. de Frutos, J. Iglesias, J. Sainz, S. Blázquez, *Microporous Mesoporous Mater.* **2005**, *86*, 364.

[19] A. Gedeon, A. Lassoued, J. Bonardet, J. Fraissard, *Microporous Mesoporous Mater.* **2001**, *44*, 801.

[20] J. D. Bass, A. Katz, *Chem. Mater.* **2003**, *15*, 2757.

[21] B. Voit, *Angew. Chem. Int. Ed.* **2006**, *45*, 4238.

[22] E. Perozo-Rondón, R. M. Martín-Aranda, B. Casal, C. J. Durán-Valle, W. N. Lau, X. Zhang, K. L. Yeung, *Catal. Today* **2006**, *114*, 183.

[23] J. Tan, X. Liu, N. Yao, Y. L. Hu, X. H. Li, *ChemistrySelect* **2019**, *4*, 2475.

[24] Y. L. Hu, Y. P. Wu, M. Lu, *Appl. Organomet. Chem.* **2018**, *32*, e4096.

[25] S. Singh, R. Kumar, H. D. Setiabudi, S. Nanda, D.-V. N. Vo, *Appl. Catal. A General* **2018**, *559*, 57.

[26] H. B. Wang, N. Yao, L. Wang, Y. L. Hu, *New J. Chem.* **2017**, *41*, 10 528.

[27] N. Yao, M. Lu, X. B. Liu, J. Tan, Y. L. Hu, *J. Mol. Liq.* **2018**, *262*, 328.

[28] T. Jin, F. Dong, Y. Liu, Y. L. Hu, *New J. Chem.* **2019**, *43*, 2583.

[29] H. Naeimi, V. Nejadshafiee, S. Masoum, *Appl. Organomet. Chem.* **2015**, *29*, 314.

[30] D. Zhao, Q. Huo, J. Feng, B. F. Chmelka, G. D. Stucky, *J. Am. Chem. Soc.* **1998**, *120*, 6024.

[31] Y. Li, W. Zhang, L. Zhang, Q. Yang, Z. Wei, Z. Feng, C. Li, *J. Phys. Chem. B* **2004**, *108*, 9739.

[32] D. Pérez-Quintanilla, I. del Hierro, M. Fajardo, I. Sierra, *Microporous Mesoporous Mater.* **2006**, *89*, 58.

[33] J. S. Sreedasyam, J. Sunkari, S. Kundha, R. R. Gundapaneni, *Acta Crystallogr.* **2013**, *E69*, o673.

[34] S. Jangra, V. Chhokar, V. K. Tomer, A. K. Sharma, S. Duhan, *J. Porous Mater.* **2016**, *23*, 1047.

[35] B. Shi, Y. Wang, Y. Guo, Y. Wang, Y. Wang, Y. Guo, Z. Zhang, X. Liu, G. Lu, *Catal. Today* **2009**, *148*, 184.

[36] Y. Liu, L. Liu, L. Kong, L. Kang, F. Ran, *Electrochim. Acta* **2016**, *211*, 469.

[37] B. J. Blackburn, J. H. Crane, C. E. Knapp, M. J. Powell, P. Marchand, D. Pugh, J. C. Bear, I. P. Parkin, C. J. Carmalt, *Mater. Des.* **2016**, *108*, 780.

[38] T. Blanquart, J. Niinistö, M. Gavagnin, V. Longo, M. Heikkilä, E. Puukilainen, V. R. Pallem, C. Dussarrat, M. Ritala, M. Leskelä, *RSC Adv.* **2013**, *3*, 1179.

[39] H. Zhu, J. Wu, M. Fang, L. Tan, C. Chen, N. S. Alharbi, T. Hayat, X. Tan, *RSC Adv.* **2017**, *7*, 36 231.

[40] F. Sordello, G. Zeb, K. Hu, P. Calza, C. Minero, T. Szkopek, M. Cerruti, *Nanoscale* **2014**, *6*, 6710.

[41] J. Safaei-Ghomi, S. H. Nazemzadeh, H. Shahbazi-Alavi, *Appl. Organomet. Chem.* **2016**, *30*, 911.

[42] J. Safaei-Ghomi, Z. Akbarzadeh, A. Ziarati, *RSC Adv.* **2014**, *4*, 16 385.